Journal of Thermal Engineering, Vol. 4, No. 2, Special Issue 7, pp. 1878-1895, February, 2018
Yildiz Technical University Press, Istanbul, Turkey

COMPUTATIONAL FLUID DYNAMICS ANALYSIS OF FLOW AND COMBUSTION OF A DIESEL ENGINE

K. Abay[1,*], U. Colak[2], L. Yüksek[3]

ABSTRACT

Efficient usage of fossil fuels and reduction of CO_2 emissions are very important priorities for the automotive industry. Without increasing contributions from diesel engines and newer diesel technologies, it would not be possible to successfully meet fuel consumption and CO_2 emission reduction targets. Therefore, new regulations and applications have been put into action to address exhaust gas emission problems. Some exhaust gases have become prominent with regard to strong effects, such as NO_x and soot. NO_x contributes to acid rain, which has deteriorating effects on the ozone layer. In this study, flow and combustion characteristics of a diesel engine are investigated by using Computational Fluid Dynamics (CFD). Whole engine components are modeled and analyses are performed for entire speed range of the engine. Calculated crank angle dependent pressure and temperature values are used as boundary condition for reactive 3D CFD simulations. Reactive CFD simulations are performed with 45° sector geometry for the period that both valves are closed. In reactive simulations, RNG k-ε and Standard k- ε models are used to characterize turbulence flow field. A lagrangian approach is used for two-phase flow computations to simulate the liquid fuel injection. Commercially available CFD code called Forte Reaction Design and its sub-module Chemkin are used for three dimensional reactive simulations, moving grid generation and problem setup. Predicted in-cylinder pressure and apparent heat release rate are validated with experimental results. NO_x and Soot formations as a result of combustion process are also investigated. Optimum level of NO_x and Soot formation obtained with 8.5% EGR usage.

Keywords: *Diesel Engine, Computational Fluid Dynamics, Exhaust Gas Recirculation, NO_x, Soot*

INTRODUCTION

The diesel engine is an internal combustion engine in which air is compressed to a sufficiently high temperature to ignite injected fuel into the cylinder. However, diesel engines seem to have some negative effects regarding emissions such as NO_x, CO, and soot [1-2]. Hence, emission control regulations have been introduced across industry sectors to avoid emissions from vehicles powered by internal combustion engines [3]. Furthermore, the demand of diesel engines increases dramatically from day to day because of their fuel efficiency and higher torque output. However, emissions are very high priorities for the automotive industry [4]. These emissions are inevitable consequences of the lower swirl ratio among diesel engines [5]. When the fluid fuel entering the combustion chamber is atomized into droplets, it vaporizes and is mixed with air, resulting a heterogeneous mixture of fuel and air. Diesel engines are generally operated with a globally lean air-fuel ratio; however, direct injection leads to different mixture regions, ranging from very lean through stoichiometry to very rich mixture ratios. Such mixture stratification inevitably causes the formation of pollutant emissions, particularly soot particles and nitrogen oxides. In addition, these emissions play a critical role in global warming and greenhouse effects. NO_x also causes acid rain and destruction of the ozone layer [6-8]. Therefore, emission control is tremendously momentous in diesel engines [9-12].

Computational fluid dynamics has a crucial importance in determining the combustion characteristics of diesel engines and the correlation between parameters leads to obtain better designs [13]. The CFD modeling of the internal combustion engines' processes has high complexity and is a challenging task, given the fact that several processes, parameters, and operating conditions within the engine should be taken into account, such as fuel injection, flame propagation, the ignition process, chemical kinetic reactions, exhaust emissions formation, tendency for knocking, and control of the air-fuel ratio. Therefore, the computation of process simulations for internal combustion engines are lengthy and require more computer memory and computing capability [14].

This paper was recommended for publication in revised form by Regional Editor Alibakhsh Kasaeian
[1]R&D Department, Turk Traktor&CNH, Ankara, TURKEY
[2]Energy Institute, Istanbul Technical University, Istanbul, TURKEY
[3]Department of Mechanical Engineering, Yıldız Technical University, Istanbul, TURKEY
**Corresponding author, E-mail address: Kurtulus.Abay@turktraktor.com.tr*
Manuscript Received 2 August 2017, Accepted 7 September 2017

In this paper, FORTE Reaction Design software, which includes Chemkin Pro-Solver, was chosen to acquire the best solution to analyze the combustion process of a diesel engine with 6 cylinders. In diesel engine models, researchers usually prefer a sector mesh for acquisition. A sector mesh can be used if the geometry is symmetrical. Two different mesh sizes have been researched, with a fine mesh giving better results than a medium mesh. The time step chosen was 1.28e-5 s during the start of injection, the duration of combustion, and the expansion stroke to minimize time decomposition. The combustion analysis examined the period between intake valve closing (IVC) and exhaust valve opening (EVO). In addition, there are a few spray models in FORTE. The spray model chosen was the radius of influence collision model (ROI) from the droplet collision and coalescence model because of its high Weber number, and catastrophic break up of fuel particles seemed to appear.

On the other hand, Chemkin was used as a chemical model to observe combustion reactions. Significantly high number of chemical reactions occurs during combustion processes and Chemkin is one of the best software packages to model these reactions. The Chemkin model consists 173 species to take better predictions. FORTE only has one soot model, called the two-step soot model [15]. When NO_x and soot emissions provide barriers in the application of diesel engines, the difficulty in dealing with the problem also comes from the trade-off feature between NO_x and soot emissions. It is always very difficult to reduce both kinds of emissions simultaneously, since factors that tend to decrease one usually increase the other. In this case, the effects of an exhaust gas recirculation rate (EGR) are researched. EGR has been investigated regarding its effects on NO_x and soot emissions as well as for determining the proper EGR rate for optimization [16].

CFD SIMULATION

The engine used for model study was a 6-cylinder, 14 liters of total cylinder volume, turbocharged direct injection diesel engine. FORTE with detailed combustion chemical kinetics in Chemkin used to investigate combustion and EGR effects. The engine properties and operating conditions are listed in Table 1 and Table 2, respectively [17].

Table 1. Engine properties

Power [kw]	91,5
Bore x Stroke [mm]	136 x 160
Compression ratio	16
Connecting rod length [mm]	304
Swirl Number	1
Valve Timing	IVC = -165° aBDC EVO = 110° bBDC
Fuel Injector Type	Common rail
Injector Hole Number	8
Injector Hole Diameter [mm]	0,196
Rail Pressure[bar]	1200
Spray Angle	152°

The engine has a bore of 136 mm and a stroke of 160 mm with a cylindrical cup piston bowl, yielding a displacement of 2.34 liters per cylinder and single swirl ration at around TDC. The engine is equipped with a non-production, high-pressure, electronically-controlled, common-rail fuel injector. For the conditions modeled here, an eight-hole, mini-sac injector cup (tip) was employed, having an angle of 152° (14° down-angle from the fire deck). The eight fuel orifices are equally spaced and have nominal diameter of 0.196 mm.

Table 2. Operating conditions

Engine speed (rpm)	1300
Temperature at Intake Valve Closing, IVC (K)	385
Pressure at Intake Valve Closing IVC (bar)	1,8
Start of Injection (dCA)	340°
Duration of Injection (dCA)	10°
Injected fuel quantity (mg/st)	0,68
EGR Rate (%)	%0
Equivalence Ratio	0,50

Chemkin with 173 species was chosen as the chemistry model. In addition, the spray properties were obtained using the radius of influence model for the droplet collision model, and the radius of influence was set at 0.2 cm. The fuel properties of $nC_{12}H_{26}$ (dodecane) were chosen, and the discharge coefficient was accepted as 0.7. The boundary conditions, such as piston temperature, head temperature, and liner temperature, were set at 500K. A sector angle of 45° was chosen, with multi-selected boundaries on which the boundary condition was applied. A sector mesh is tremendously useful in constituting a much smaller mesh size. Different turbulence models and mesh sizes were used in the simulation to observe their effects on the combustion outputs.

In FORTE, two mesh sizes 50,000 and 500,000 are preferred and were compared to the experimental data, such as to pressure and heat release. Fine mesh is closer to the experimental data compared to medium mesh. Thereafter, turbulence models such as RNG k-epsilon and Standard k-epsilon were compared and the closer turbulence model to experimental result in terms of in cylinder pressure was chosen. The sector mesh, which is a fine mesh size at top dead center (TDC) is shown Figure 1a and at bottom dead center (BDC), is illustrated in Figure 1b. Injector location is demonstrated in Figure 2.

Turbulence kinetic energy for Standard k-epsilon turbulence model is shown below [18];

$$\frac{\partial}{\partial t}(\rho k)+\frac{\partial}{\partial x_j}\left[\rho u_j k-\left(\mu+\frac{\mu_t}{\sigma_k}\right)\frac{\partial k}{\partial x_j}\right]=\mu_t\left(S_{ij}\frac{\partial u_i}{\partial x_j}-\frac{g_i}{\sigma_{h,t}}\frac{1}{\rho}\frac{\partial \rho}{\partial x_i}\right)-\rho\varepsilon-\frac{2}{3}\left(\mu_t\frac{\partial u_i}{\partial x_i}+\rho k\right)\frac{\partial u_i}{\partial x_i} \quad (1)$$

Turbulent dissipation for Standard k-epsilon turbulence model is shown;

$$\frac{\partial}{\partial t}(\rho\varepsilon)+\frac{\partial}{\partial x_j}\left[\rho u_j\varepsilon-\left(\mu+\frac{\mu_t}{\sigma_\varepsilon}\right)\frac{\partial \varepsilon}{\partial x_j}\right]=\ldots$$

$$\ldots C_{e1}\frac{\varepsilon}{k}\left[\mu_t S_{ij}\frac{\partial u_i}{\partial x_j}-\frac{2}{3}\left(\mu_t\frac{\partial u_i}{\partial x_i}+\rho k\right)\frac{\partial u_i}{\partial x_i}\right]-C_{e2}\rho\frac{\varepsilon^2}{k}-C_{e3}\frac{\varepsilon}{k}\mu_t\frac{g_i}{\sigma_{h,t}}\frac{1}{\rho}\frac{\partial \rho}{\partial x_i}+C_{e4}\rho\varepsilon\frac{\partial u_i}{\partial x_j} \quad (2)$$

ρ, k, ε, u, σ, S_{ij} expresses density, turbulent kinetic energy, turbulent dissipation rate, absolute velocity, turbulence Prandtl number and average tension rate, respectively. With regard to $C_{e1}, C_{e2}, C_{e3}, C_{e4}$ coefficients, the values of them are listed Table 3 [19].

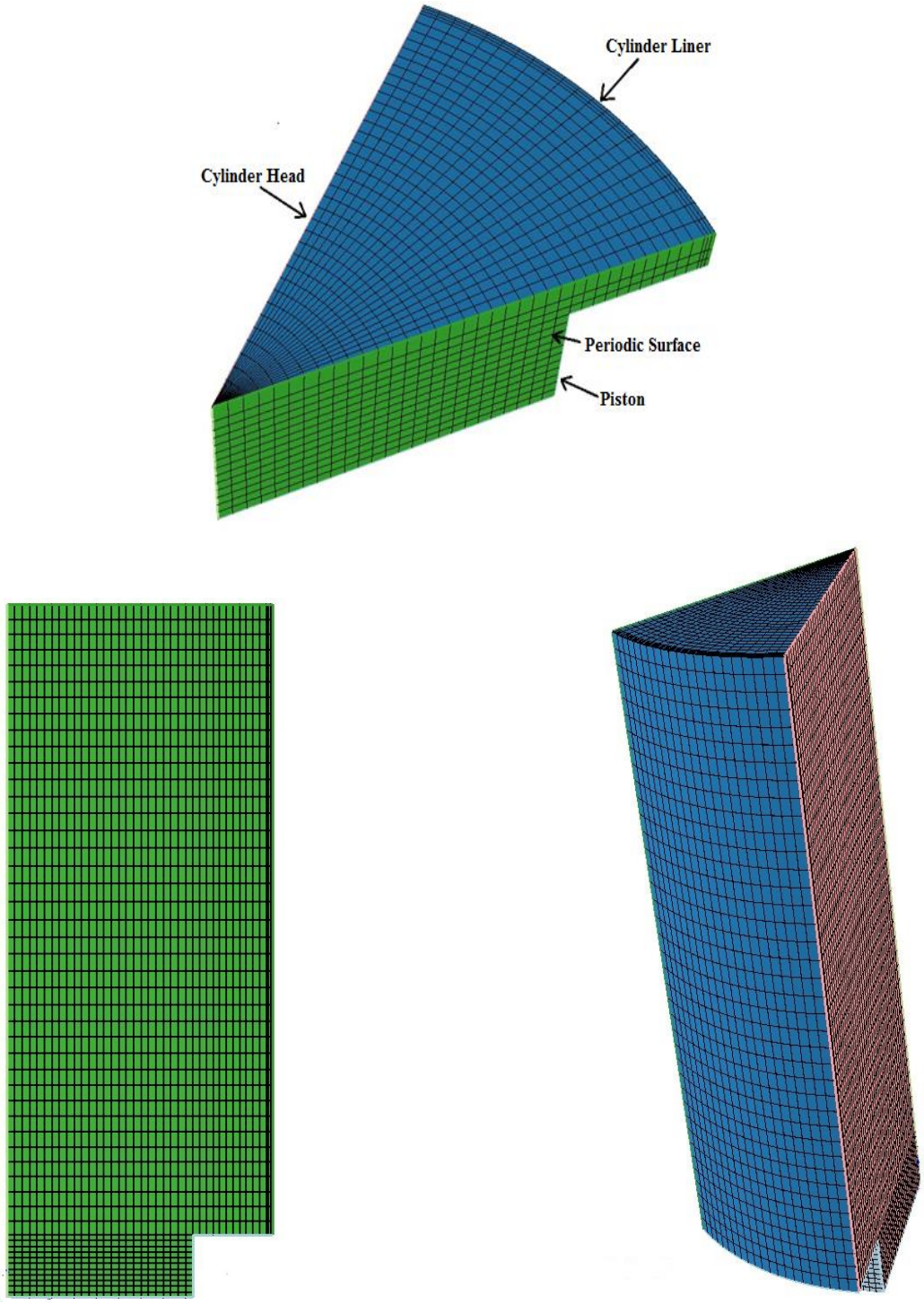

(a) (b)

Figure 1. Sector mesh at (a) TDC, (b) BDC.

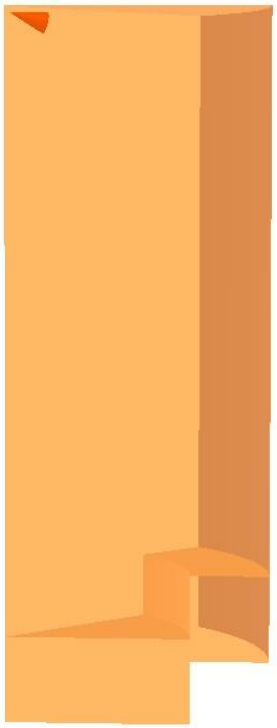

Figure 2. Injector location in the cylinder

Table 3. Standard k-epsilon Turbulence Model Coefficients

C_μ	σ_k	σ_ϵ	$C_{\epsilon 1}$	$C_{\epsilon 2}$	$C_{\epsilon 3}$	$C_{\epsilon 4}$	K
0.09	1	1.22	1.44	1.92	1.44	-0.33	0.419

Furthermore, there is a difference in turbulent dissipation between Standard k-epsilon and RNG k-epsilon. Turbulent dissipation and coefficients for RNG k-epsilon turbulence model is shown [20];

$$\frac{\partial}{\partial t}(\rho\varepsilon)+\frac{\partial}{\partial x_j}\left[\rho u_j\varepsilon-\left(\mu+\frac{\mu_t}{\sigma_\varepsilon}\right)\frac{\partial\varepsilon}{\partial x_j}\right]=\cdots$$

$$\ldots=C_{e1}\frac{\varepsilon}{k}\left[\mu_t S_{ij}\frac{\partial u_i}{\partial x_j}-\frac{2}{3}\left(\mu_t\frac{\partial u_i}{\partial x_i}+\rho k\right)\frac{\partial u_i}{\partial x_i}\right]-C_{e2}\rho\frac{\varepsilon^2}{k}-C_{e3}\frac{\varepsilon}{k}\mu_t\frac{g_i}{\sigma_{h,t}}\frac{1}{\rho}\frac{\partial\rho}{\partial x_i}+C_{e4}\rho\varepsilon\frac{\partial u_i}{\partial x_j}-\frac{C_\mu\eta^3\left(1-\eta/\eta_0\right)}{1+\beta\eta^3}\frac{\rho\varepsilon^2}{k} \quad (3)$$

RNG k-epsilon turbulence model coefficients are listed in Table 4.

Table 4. RNG k-epsilon Turbulence Model Coefficients

C_μ	σ_k	σ_ϵ	σ_h	σ_m	$C_{\epsilon 1}$	$C_{\epsilon 2}$	$C_{\epsilon 3}$	$C_{\epsilon 4}$	K	E
0.085	1	1.22	0.9	0.9	1.42	1.68	1.44	-0.33	0.4	9

Rate of heat release was calculated by means of in-cylinder pressure and then compared to the experimental results according the formulae given below.

$$\frac{dQ}{dCA}=\frac{\gamma}{\gamma-1}p\frac{dV}{dCA}+\frac{1}{\gamma-1}V\frac{dp}{dCA} \quad (4)$$

Q is the total amount of heat released; dQ/dCA is the heat release per crank angle as J/dCA, V is the cylinder instantaneous volume, p is the cylinder pressure, and γ is the ratio of specific heats. The experimental

data was obtained by Singh et al.'s study [17] where the test engine is equipped with a non-production, high-pressure, electronically-controlled, common-rail fuel injector.

RESULTS AND DISCUSSION

The pressure and rate of heat release values were compared with the experimental results. The differences connected to in-cylinder pressure between fine mesh, medium mesh and experiment are illustrated in Figure 3. Two mesh sizes were implemented to assess the accuracy of the CFD model. The difference between fine mesh and experiment in terms of pressure values was approximately 6.66%. On the other hand, there can be seen 4% difference between fine mesh and experimental. Therefore, CFD analysis was continued with a fine mesh. Figure 3a shows a good comparison of the results between the predicted and measured in-cylinder pressure curves.

The difference between the model and experimental curves related to rate of heat release is indicated in Figure 3b. The effect of the pressure difference between the model and measured data on the rate of heat release is clearly demonstrated. Although the pressure difference at the beginning of ignition between the model and experimental curves is low, the differences in rate of heat release between the model and experimental curves are much higher.

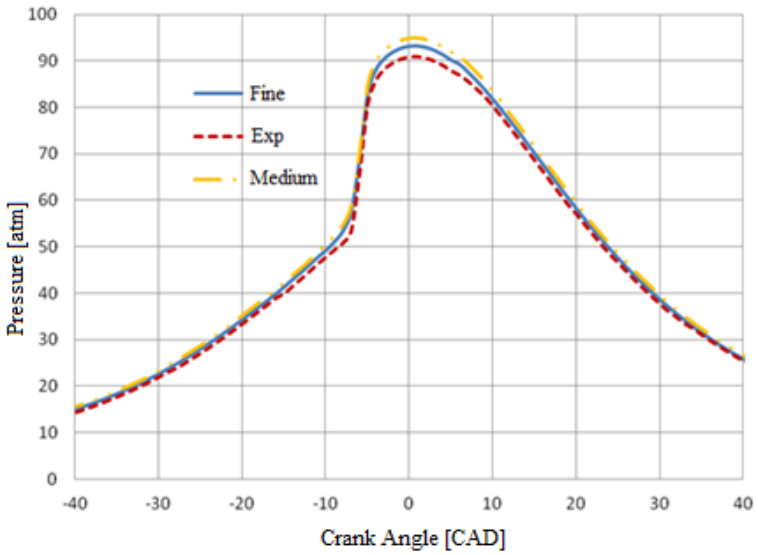

(a)

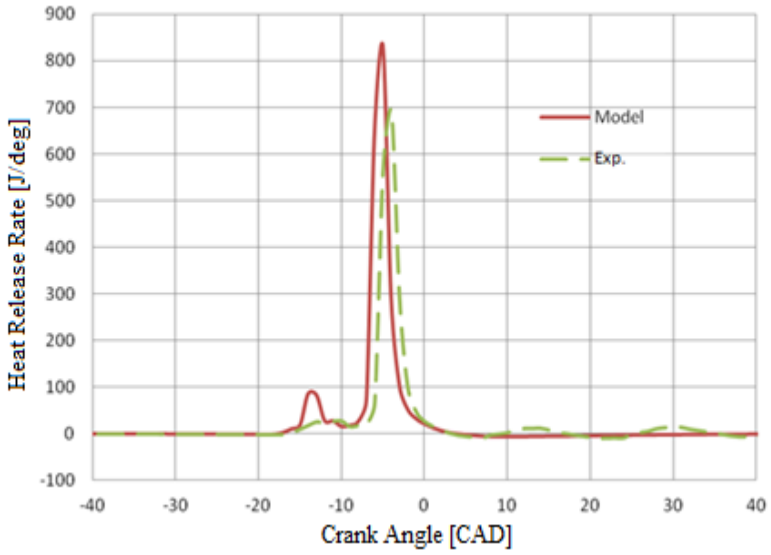

(b)

Figure 3. The comparison of medium, fine mesh and experimental result for (a) cylinder pressure and (b) Rate of heat release

The average and maximum temperature curves in the cylinder are shown in Figure 4a and 4b, respectively.

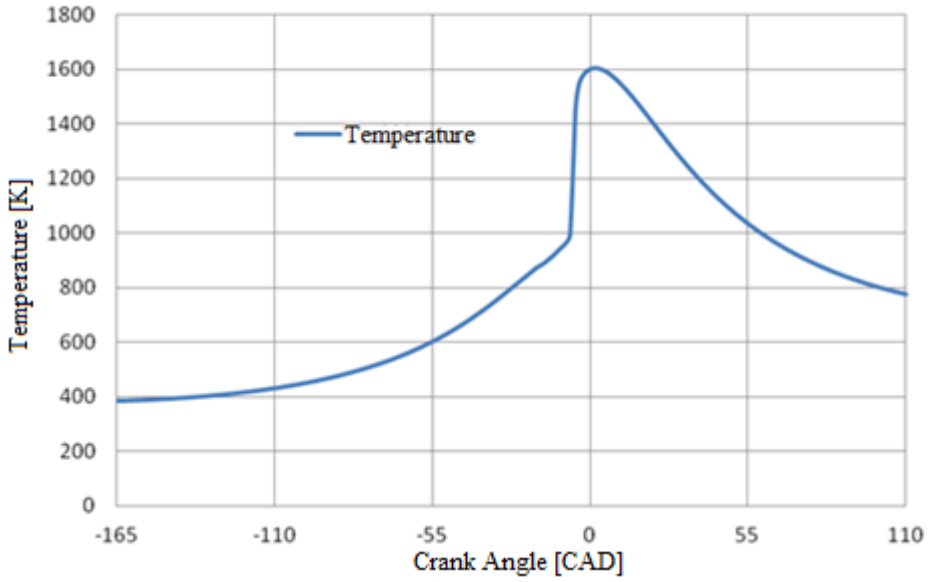

(a)

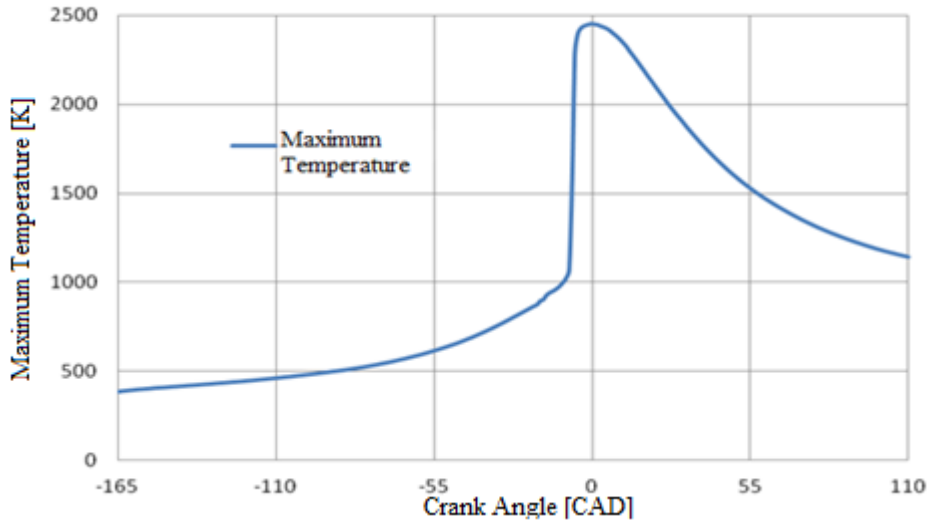

(b)

Figure 4. Variation of (a) average and (b) maximum temperature.

Three types of injection were modeled in this study which are early, standard, and late. If the start of injection in a diesel engine is between −30° and −12 ° CA, then it is called an early injection. If the start of injection is between −12° and 0° CA, it is called standard injection, and if the start of injection is between 0° and 15° CA, it is called late injection. The advantage of early injection is associated with homogeneous mixtures. This is particularly important, since there is not enough time for diesel engines to obtain a homogenous gas and fuel mixture [21-23].

Figure 4a shows that −7° CA is acceptable as the ignition time. The characteristic of the curve appears to be like that of a compression ignition engine due to the early injection. Figure 5 illustrates the fuel particles and in-cylinder temperature contour from the start of injection to the piston location at the TDC. The fuel particles' vaporization, ignition, and combustion are clearly shown. Initially, the fuel particles' temperature started to rise from the beginning of the injection, and then the fuel particles started to vaporize. As a result of the fuel particles' vaporization, gases in the cylinder and fuel vapor constitute homogenous mixture. Ultimately, as a consequence

of the fuel and gas mixing, ignition is carried out and combustion begins. Furthermore, piston displacement to the TDC is shown in Figure 5.

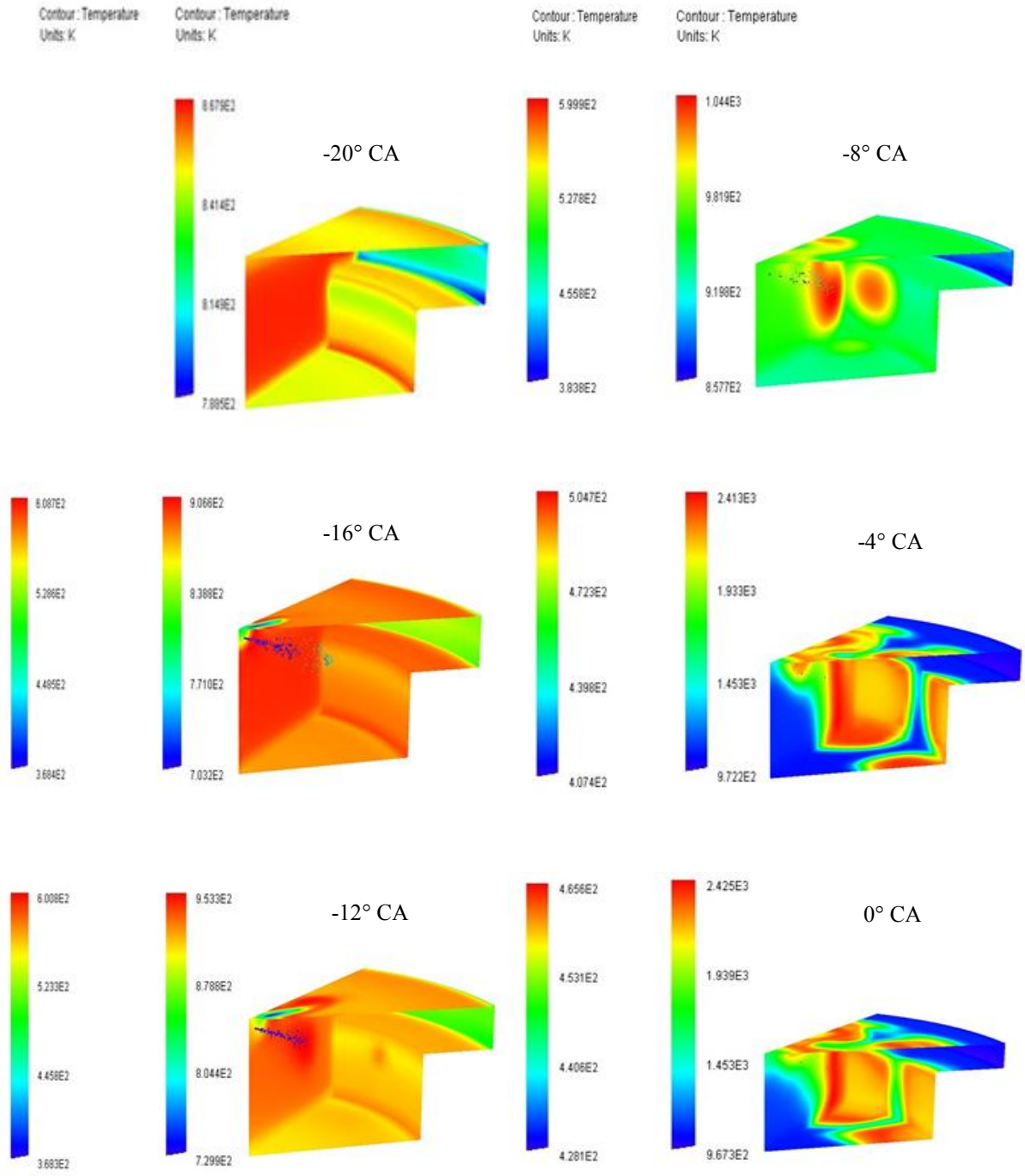

Figure 5. Fuel particles and in cylinder temperature contours.

There are two turbulence model types in FORTE: RNG k-epsilon and standard k-epsilon. The RNG k-epsilon is generally preferred for internal combustion engine simulations because of its better calibration than the standard k-epsilon turbulence model. The RNG k-ε and Standard k-ε turbulence models are generally preferred if the Reynolds number is high [23].

Figure 6a summarizes the difference in the pressure curves between the RNG and standard k-epsilon turbulence models, and it can be seen that the RNG k-epsilon turbulence model is closer to the experimental

pressure curve. Therefore, the RNG k-epsilon model was used as the turbulence model in this analysis. Figure 6b indicates velocity distribution with respect to turbulence models.

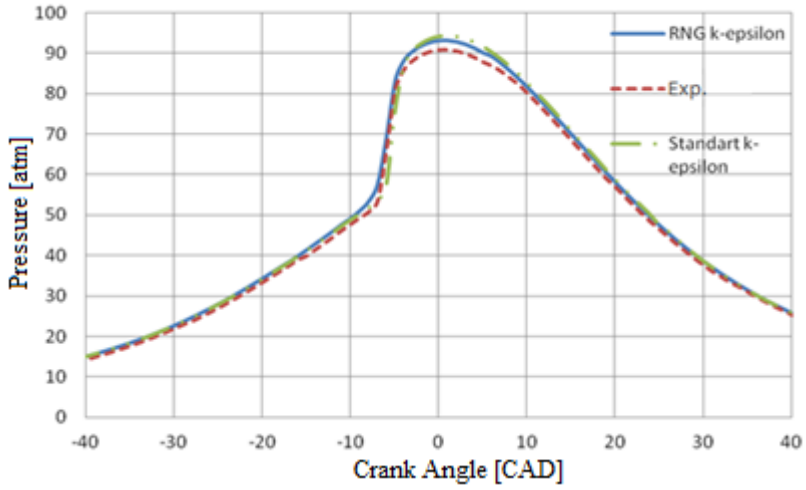

(a)

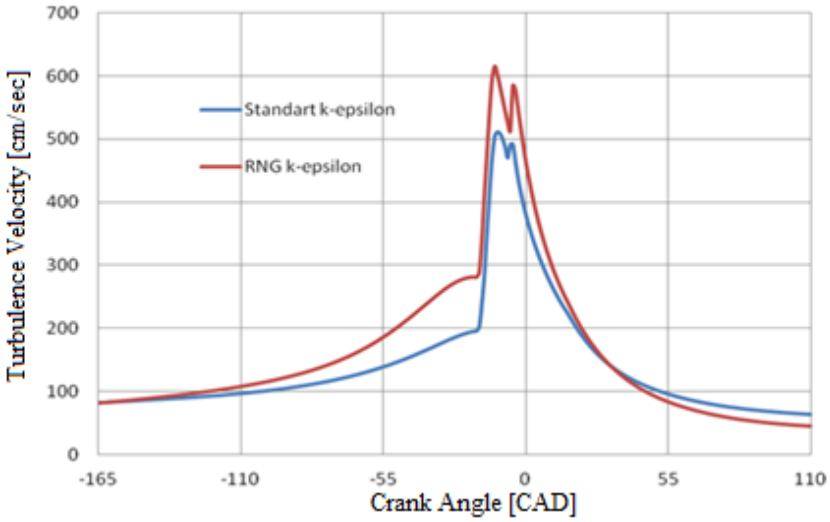

(b)

Figure 6. Variation of the turbulence models for (a) pressure and (b) velocity.

EGR is a method of decreasing NO_x emissions by introducing exhaust gas into the combustion chamber. NO_x emerges at areas with rich oxygen and sufficiently high temperature. For this reason, EGR provides exhaust gas species such as N_2, CO_2, and H_2O to the combustion chamber to decrease the oxygen concentration [24-26]. In this case, the combustion lasts longer than before and the rate heat of release drops. Moreover, the specific heats of exhaust gases such as CO_2 and H_2O are higher than that of intake air [28-31]. In addition, this higher specific heat mixture leads to lower combustion temperature, so that NO_x emissions reduce dramatically due to decrease in-cylinder temperature [31-32].

The amount of composed NO in the cylinder for the duration of combustion can be seen in Figure 7a according to the different EGR rates. As the EGR rates increase, the composed NO amounts in the cylinder fall significantly. After a characteristic rate, EGR method loses its' affectivity for NO_x reduction. In Figure 7a, the difference between having an EGR system and not having one was 5%. This difference decreases when EGR rates increase, especially after the 15% EGR rate. In Figure 7a the maximum temperature difference is approximately 286K.

A number of negative effects are connected to EGR, such as increased amount of soot and decreased power. High temperatures result in soot particles being combusted in cylinder, so EGR leads to a significantly increased amount of soot due to the fall of maximum temperature. Soot distribution in reference to EGR rates is illustrated in Figure 7b.

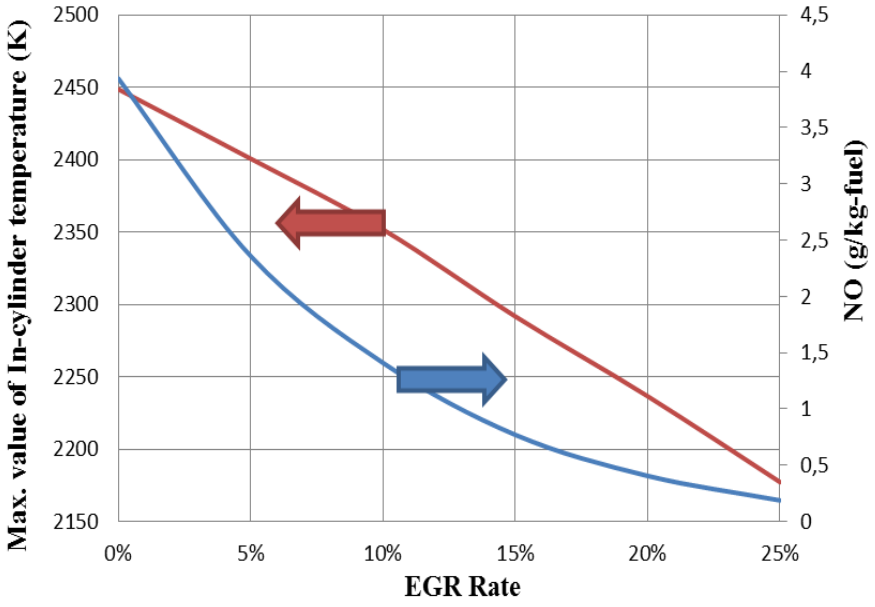

(a)

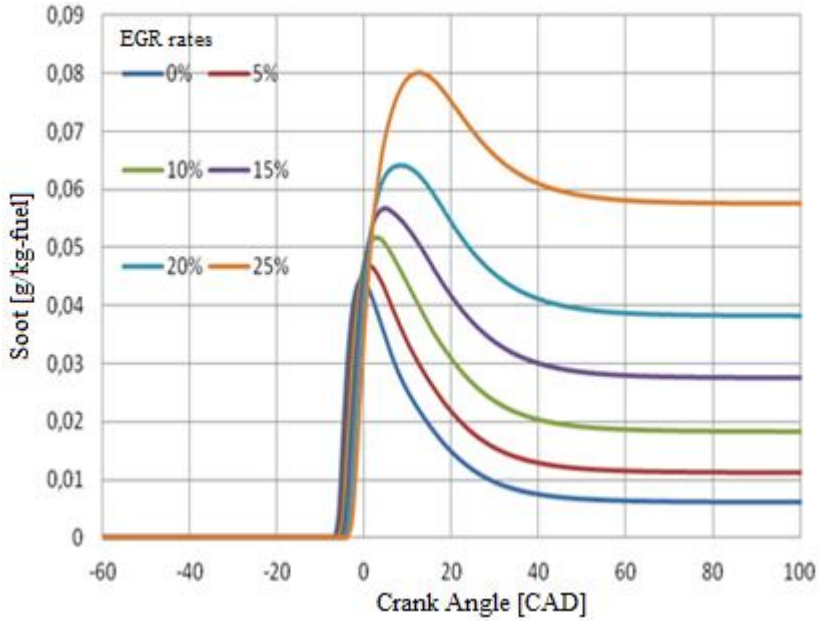

(b)

Figure 7. Detailed comparisons of (a) NO/maximum temperature and (b) soot with different EGR rates

Figure 8 shows the amount of soot according to different EGR rates with decreasing maximum in-cylinder temperature.

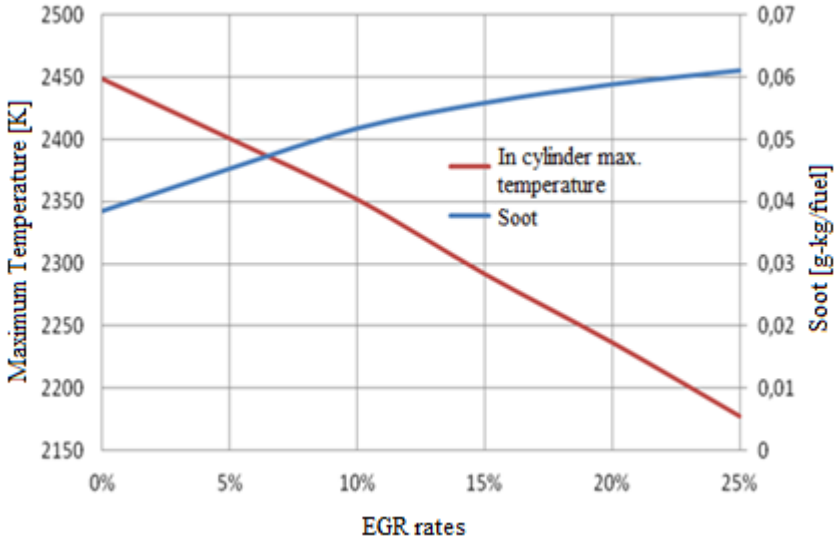

Figure 8. Soot variation with maximum temperature in terms of different EGR rates

As the EGR rate increase the maximum in-cylinder temperatures are tend to decrease as shown in Figure 9. This is particularly important, since engine performance is directly affected by the maximum in-cylinder temperature.

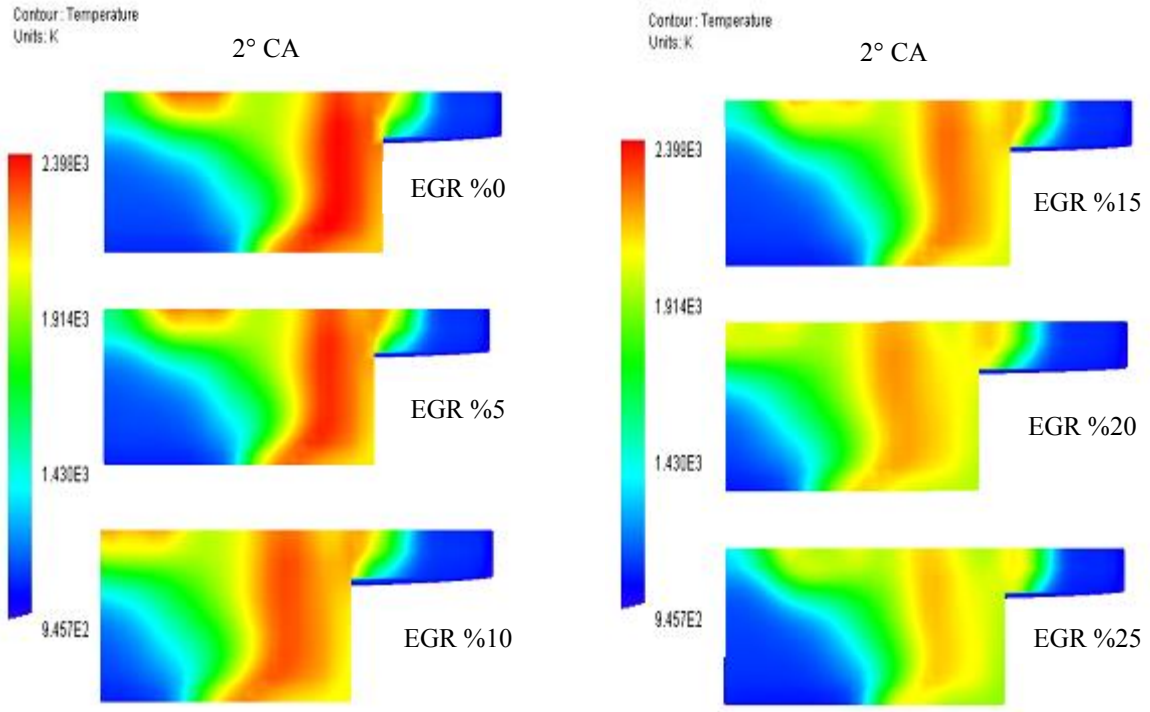

Figure 9. In cylinder maximum temperatures with different EGR rates

Variation of the engine power can be seen in Figure 10 with respect to the EGR rate. In Figure 11, trends in NO and soot are demonstrated with different EGR rates.

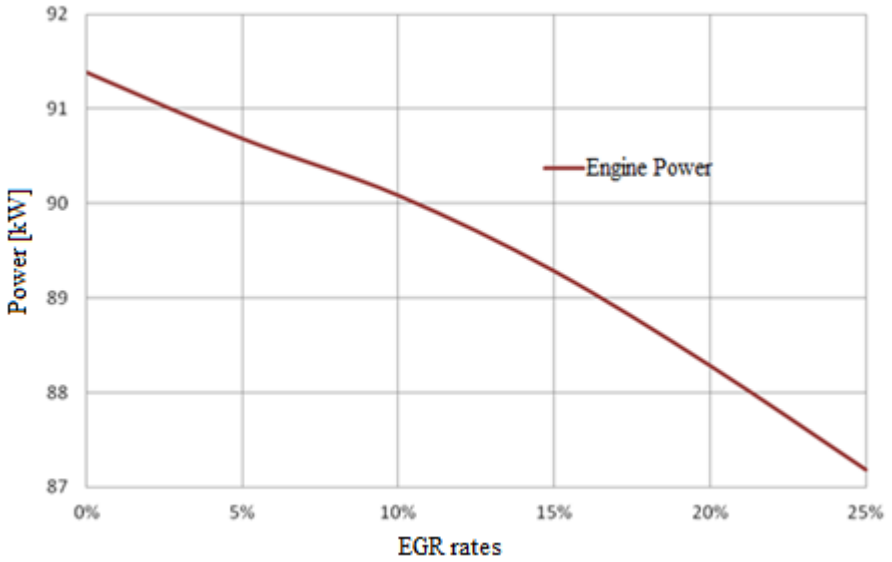

Figure 10. Power change according to the different EGR rates

Using the correct EGR rate is particularly important in terms of engine performance, soot and NO_x emissions. As a result, the correct EGR rate for this engine is 8.5%, which is the trade-off value of NO and soot in Figure 11.

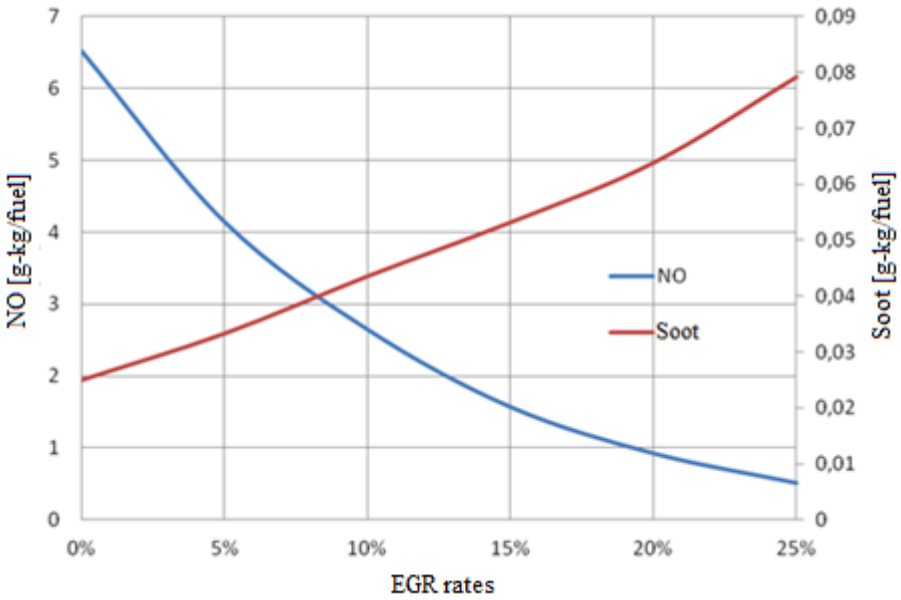

Figure 11. NO and Soot change with different EGR rates

The sector mesh was completed for the full combustion chamber, and its contours during the injection are shown in Figure 12.

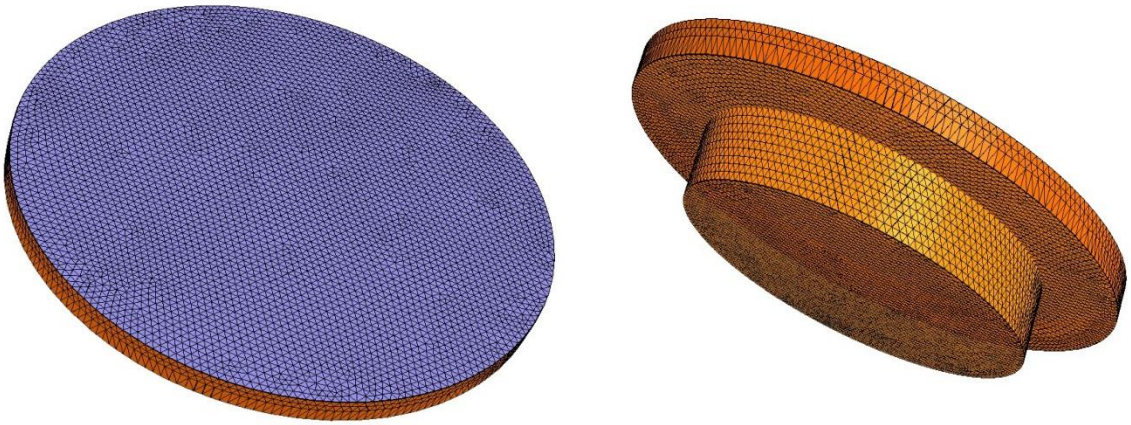

Figure 12. Full Combustion chamber

In Figure 13, the injection phases and temperature of fuel particles are shown on piston bowl. Nozzles of an injector can be seen along with the temperature distributions. Fuel particles started to vaporize as a result of temperature rise. The distribution of fuel particles in the cylinder was homogenous during injection.

(a)

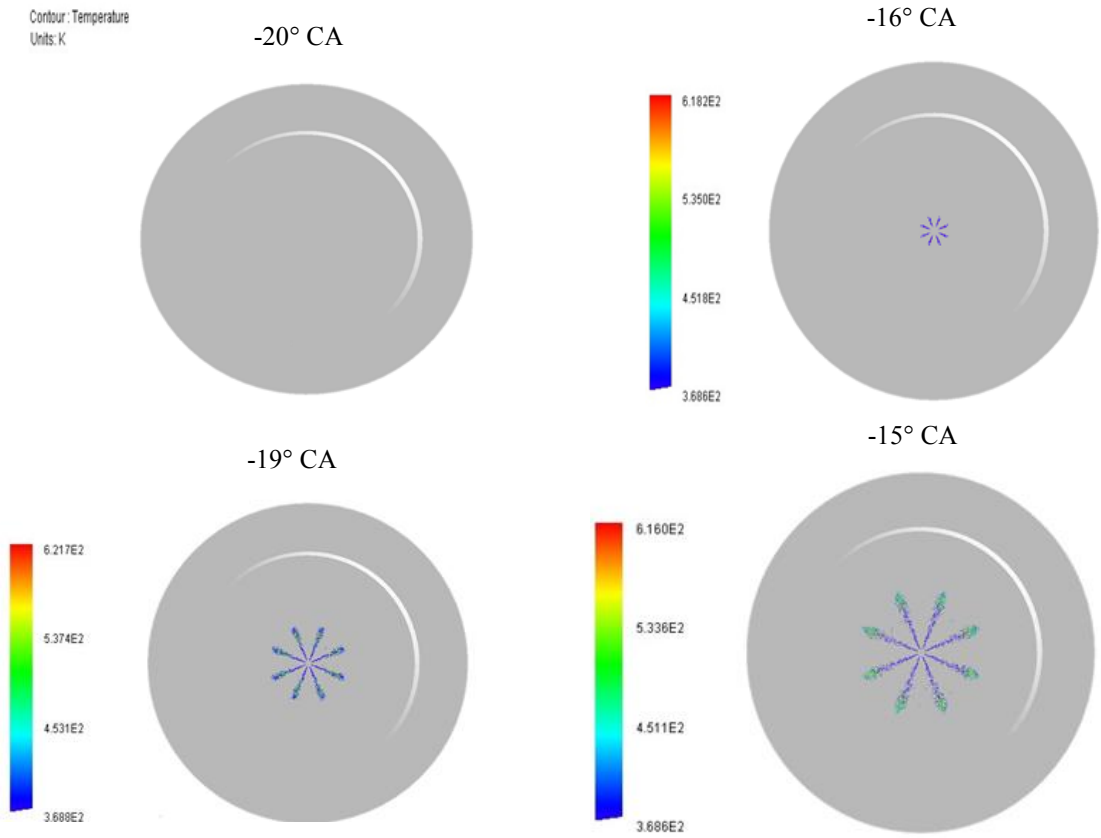

-18° CA

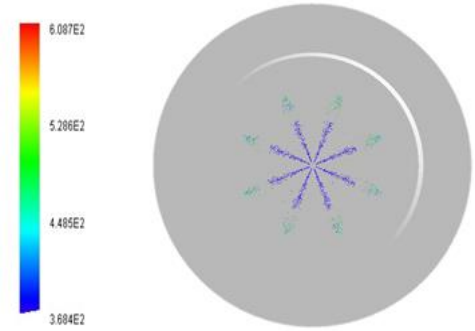

-14° CA

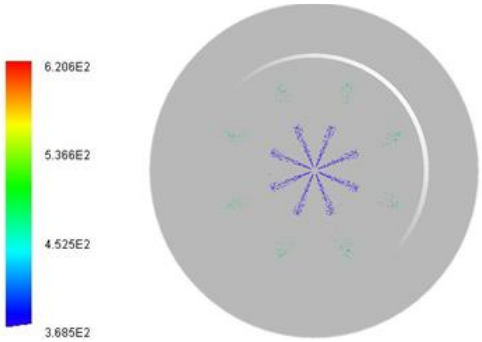

-17° CA

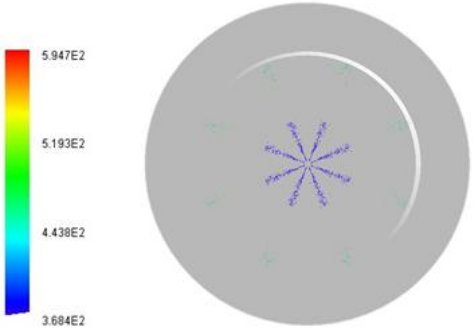

-13° CA

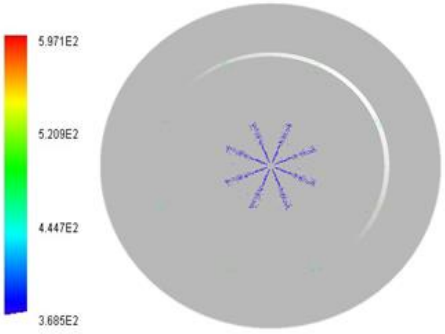

-12° CA

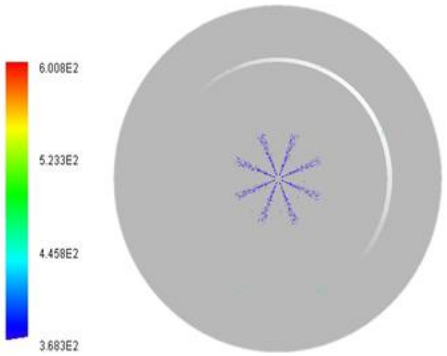

-11° CA

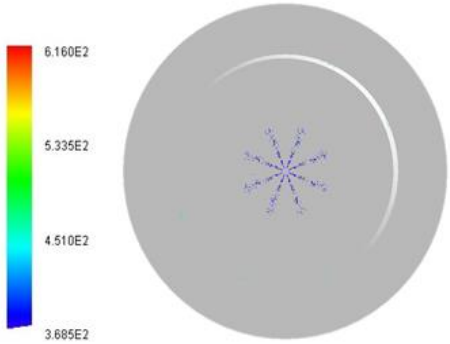

(b)

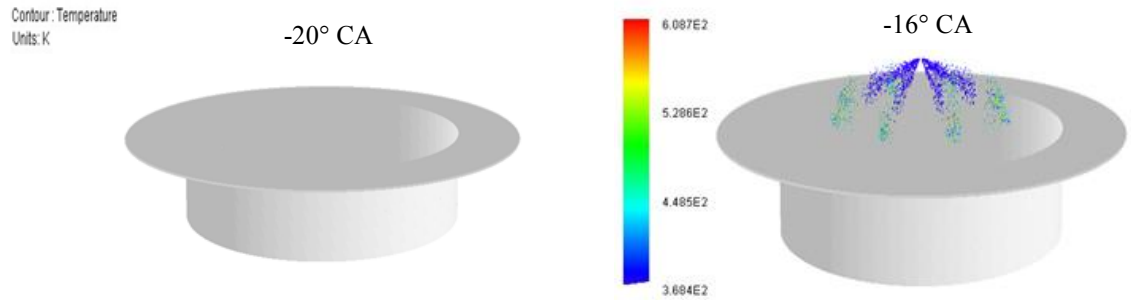

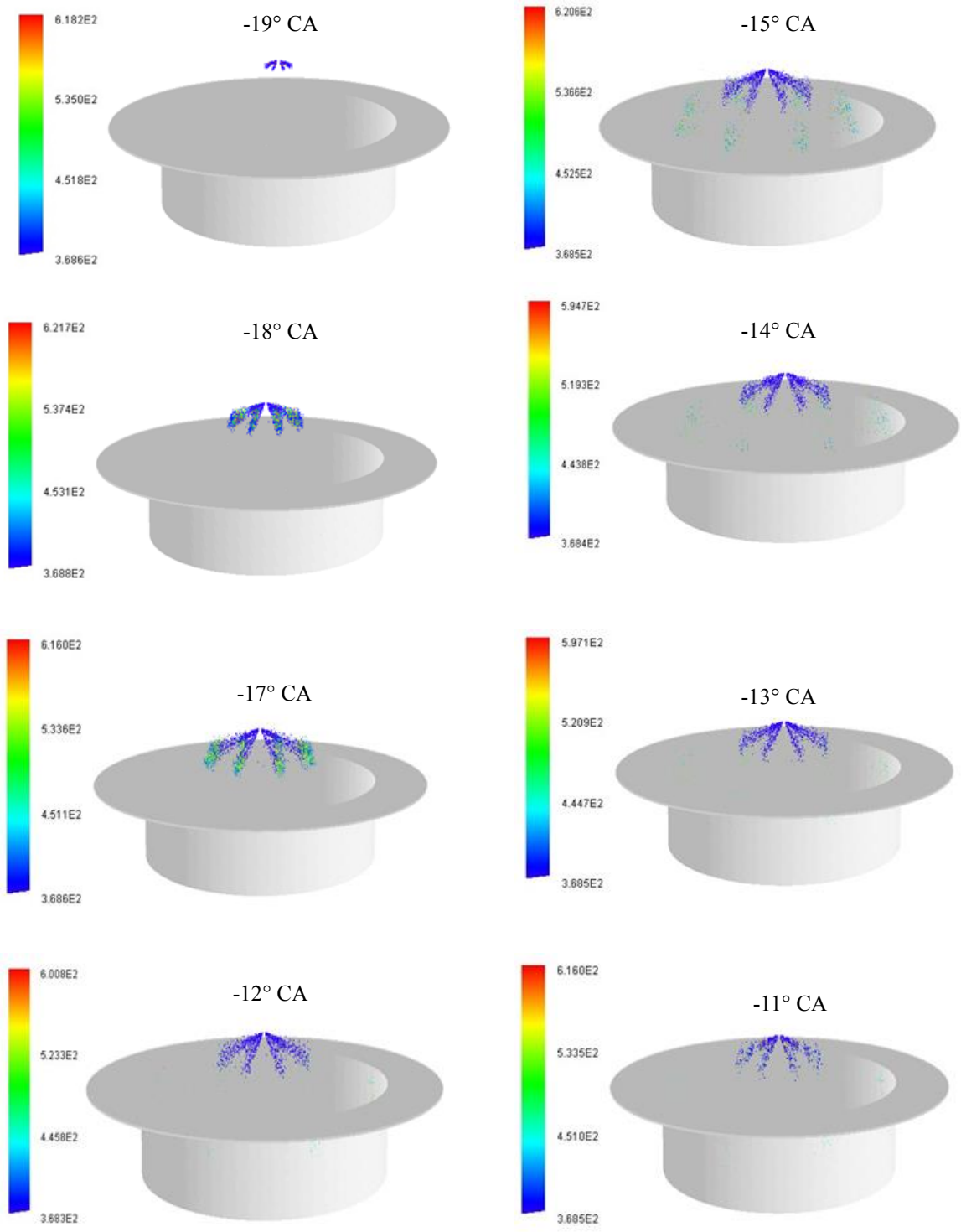

Figure 13. Particle distribution on piston bowl during injection. (a) for vertical and (b) for horizontal.

CONCLUSION

In this paper, combustion simulation of a diesel engine was performed by using CFD. A 6-cylinder, 14-liters of total cylinder volume, turbocharged diesel engine was simulated using FORTE Reaction Design and Chemkin Pro Solver. The results of this engine combustion were compared to the experimental data in terms of in cylinder pressure and heat release.

A set of simulations were performed for diesel combustion using a sector mesh. Piston and injector geometry were modeled as eight-point reactive sector simulation during the valves are closed. Mesh, time stepping and turbulence modeling are performed to this partial section. Two different mesh sizes were used, with application

of the fine mesh better results are obtained compared to the medium mesh. Furthermore, RNG k-ε turbulence and Standard k-ε turbulence models were used to compare the combustion results in this work, which showed that the results of the CFD analysis using the RNG k-ε turbulence model were closer to the experimental data than those of the Standard k-ε turbulence model because it is more advantageous than the standard k-ε turbulence model in predicting small eddies and is better calibrated. Liquid fuel evaporation and spray formation were analyzed by the Lagrangian method. The average in-cylinder pressure values and the rate of heat released are compared with experimental results and verified. According to the average cylinder pressure results, there is a 4% difference between the experiment and CFD results.

In addition, the effect of the EGR percentage on the NO and soot mass ratios that were produced after combustion was investigated. In parallel with the increase in EGR, it was observed that the temperature in the cylinder and the amount of formed NO decreased. The resulting mass of soot has increased in reverse proportion with NO.

The optimum EGR considering the soot and NO_x was considered as 8.5%, which is the optimal value for 1300 rpm. It is seen that the results of reactive three-dimensional simulation with the whole engine model are close to the sector results. For this reason, analyzes such as combustion and spray formation can be obtained with high accuracy by sector simulations considering the computer processing time. By incorporating intake and exhaust strokes, the character of the air taken into the cylinder and its effect on the fuel-air mixture can be examined.

NOMENCLATURE

E	Energy
ρ	Density
P	Power
V	Volume
A	Area
CFD	Computational Fluid Dynamics
EGR	Exhaust Gas Recirculation
BDC	Bottom Dead Center
TDC	Top Dead Center
dCA	Crank Angle Degree

REFERENCES

[1] Patil, K. R., & Thipse, S. S. (2015). Experimental investigation of CI engine combustion, performance and emissions in DEE-kerosene-diesel blends of high DEE concentration. Energy Conversion and Management, 89, 396–408.

[2] Rakopoulos, C. D., & Giakoumis, E. G. (2009). Diesel engine transient operation: Principles of operation and simulation analysis. Diesel Engine Transient Operation: Principles of Operation and Simulation Analysis.

[3] Karimi, K. (2007). Characterisation of Multiple-Injection Diesel Sprays at Elevated Pressures and Temperatures. University of Brighton.

[4] Merker, G. P., Schwarz, C., Stiesch, G., & Otto, F. (2005). Simulating combustion: simulation of combustion and pollutant formation for engine-development. Springer Science & Business Media.

[5] Timoney, D. J., & Smith, W. J. (1996). Influences of Fuel Injection and Air Motion Energy Sources on Fuel-Air Mixing Rates in a D . I . Diesel Combustion System. Papers\SAE Papers\Diesel 1990-2002, (412).

[6] Hong, Y. K., Lee, D. W., Ko, Y. C., Yinghua, L., Han, H. S., & Lee, K. Y. (2010). Passive NOxreduction with CO using Pd/TiO2/Al2O3+ WGSR catalysts under simulated post-euro IV diesel exhaust conditions. Catalysis Letters, 136(1–2), 106–115.

[7] Innes, W. B. (1981). Effect of nitrogen oxide emissions on ozone levels in metropolitan regions. Environmental science & technology, 15(8), 904-912.

[8] Mills, A., & Elouali, S. (2015). The nitric oxide ISO photocatalytic reactor system: Measurement of NOxremoval activity and capacity. Journal of Photochemistry and Photobiology A: Chemistry, 305, 29–36.

[9] Rakowski, I. S., & Eckert, I. P. (2012). Engine Combustion. In Combustion Engines Development (pp. 119-168). Springer Berlin Heidelberg.

[10] Liu, Y. (2003). Diesel engine modeling and optimization for emission reduction.

[11] Fuchs, T. R., & Rutland, C. J. (1998). Intake flow effects on combustion and emissions in a diesel engine (No. 980508). SAE Technical Paper.

[12] Miles, P. C. (2000). The influence of swirl on HSDI diesel combustion at moderate speed and load (No. 2000-01-1829). SAE Technical Paper.
[13] Zellat M., Abouri D., Duranti S., (2007). Recent Advances in Diesel Combustion Modeling. 17th International Multidimensional Engine User's meeting at the SAE Congress, Detroit.
[14] Kurniawan, W. H., & Abdullah, S. (2008). Numerical analysis of the combustion process in a four-stroke compressed natural gas engine with direct injection system. Journal of mechanical science and technology, 22(10), 1937-1944.
[15] FORTE Reaction Design (2014). Forte Theory Manual, pp. 11-14.
[16] Heywood, J. B. (1988). Internal combustion engine fundamentals (Vol. 930). New York: Mcgraw-hill.
[17] Singh, S., Reitz, R. D., & Musculus, M. P. (2006). Comparison of the characteristic time (CTC), representative interactive flamelet (RIF), and direct integration with detailed chemistry combustion models against optical diagnostic data for multi-mode combustion in a heavy-duty DI diesel engine (No. 2006-01-0055). SAE Technical Paper.
[18] Combustion Models against Optical Diagnostic Data for Multi-Mode Combustion in a Heavy-Duty DI Diesel Engine (2006) SAE Paper No. 2006-01-055, Detroit, Michigan, April.
[19] Munnannur, A. (2007). Droplet collision modeling in multi-dimensional engine spray computations (Vol. 68, No. 12).
[20] Bari, S., Yu, C. W., & Lim, T. H. (2004). Effect of fuel injection timing with waste cooking oil as a fuel in a direct injection diesel engine. Proceedings of the Institution of Mechanical Engineers, Part D: Journal of Automobile Engineering, 218(1), 93-104.
[21] Karthik, T. S. D. (2011). Turbulence models and their applications. 10th Indo German Winter Academy, 1–52.
[22] Lee, Y., & Huh, K. Y. (2014). Analysis of different modes of low temperature combustion by ultra-high EGR and modulated kinetics in a heavy duty diesel engine. Applied Thermal Engineering, 70(1), 776-787.
[23] Pandian, M., Sivapirakasam, S. P., & Udayakumar, M. (2010). Investigations on emission characteristics of the pongamia biodiesel-diesel blend fuelled twin cylinder compression ignition direct injection engine using exhaust gas recirculation methodology and dimethyl carbonate as additive. Journal of Renewable and Sustainable Energy, 2(4).
[24] Güney H. (2014). Tier IV Emisyon Seviyesine Sahip Bir Dizel Motorun Hesaplamalı Akışkanlar Dinamiği ile Akış ve Yanma Analizi. (Graduate dissertation).
[25] Yakhot, V., & Orszag, S. A. (1986). Renormalization group analysis of turbulence. I. Basic theory. Journal of scientific computing, 1(1), 3-51.
[26] Hiroyasu, H., & Kadota, T. (1976). Models for combustion and formation of nitric oxide and soot in direct injection diesel engines (No. 760129). SAE Technical Paper.
[27] Vishwanathan, G., & Reitz, R. D. (2008). Numerical predictions of diesel flame lift-off length and soot distributions under low temperature combustion conditions (No. 2008-01-1331). SAE Technical Paper.
[28] Zhao, H., Peng, Z., Williams, J., & Ladommatos, N. (2001). Understanding the effects of recycled burnt gases on the controlled autoignition (CAI) combustion in four-stroke gasoline engines (No. 2001-01-3607). SAE Technical Paper.
[29] Law, D., Allen, J., & Chen, R. (2002). On the mechanism of controlled auto ignition.
[30] Law, D., Kemp, D., Allen, J., Kirkpatrick, G., & Copland, T. (2001). Controlled combustion in an IC-engine with a fully variable valve train (No. 2001-01-0251). SAE Technical Paper.
[31] Kong, S. C., & Reitz, R. D. (2002). Use of detailed chemical kinetics to study HCCI engine combustion with consideration of turbulent mixing effects. Journal of engineering for gas turbines and power, 124(3), 702-707.
[32] Colannino, J. (2006). Modeling of combustion systems: A practical approach. CRC Press.